Chapter

Boiling Heat Transfer on the Micro-Textured Interfaces

Tatsuhiko Aizawa, Naoki Ono and Hiroki Nakata

Abstract

Higher heat flux than its normal criticality from high-power transistors, LIDAR (Laser Imaging Detection and Ranging), stacked CPUs, high-power transistors, and lasers must be efficiently transferred to cooling media through the metallic interface. The micro-/nano-textured aluminum and copper devices were highlighted among several approaches and fabricated to enhance the boiling heat transfer process to the subcooled water. The plasma printing was proposed to fabricate a pure aluminum device with concave micro-textures and to describe the boiling heat transfer behavior with comparison to the bare aluminum plate. A copper device was wet-plated to have convex micro-textures and to discuss the effect of micro-textures on the heat transfer characteristics under the forced water cooling by varying the Reynolds number. The boiling curve on the micro-textured interfaces was newly constructed by improving the boiling heat transfer process by micro-/nano-texturing.

Keywords: boiling heat transfer, micro-/nano-texturing, aluminum, copper, boling curve, critical heat flux (CHF), superheat, micro-bubbles, Reynolds number

1. Introduction

High-performance forced cooling in VLSI (Very-Large-Scale Integrated) circuits [1] became a turning point to reconsider how to improve the capacity to cool down the highly energy-consuming devices and systems. Since then, various efforts were reported on the heat and mass transfer engineering. Micro-fluid channel heat sink in a single phase was proposed to improve the heat transfer from the heated surface to the cooling media. As surveyed in [2–4], numerical simulations were performed to optimize the micro-channel network. Various computational models were developed to control the heat transfer process [5]. The experimental works followed these theoretical discussions to enhance the boiling heat transfer with the use of porous interface [6]. Those studies insisted that thermal spreading with high heat flux could never be installed in practice without innovative modification in heat and mass transfer process.

In general, there are several heat transfer processes with and without phase transformation; e.g., the natural flow convection, the forced flow convection, and the boiling heat transfer. Among them, the boiling heat transfer process provides the highest heat flux condition in practice [7]. Toward the innovation in the boiling heat

transfer technologies, the heat and mass transfer mechanism with phase transformation must be reconsidered to modify a boiling curve. In this chapter of book on the heat transfer, several new ideas were discussed to control the heat and mass transfer; e. g., a micro-porous interface design in [6], a micro-structured surface design via the spray cooling [8], a micro-/nano-scale surface modification [9, 10], and wettability-controlled surface design [11]. They provided a possibility to attain higher heat flux than the critical heat flux (CHF) limit [7]. In addition, the nanoscale morphology of heat-dissipating media became important to enhance the heat transfer on the heating surface even with phase transformation [12]. Those studies suggest the importance of the boiling curves on the micro-/nano-textured interface between the heating metallic solid and the cooling media.

After [7], three engineering items must be considered to describe the heat transfer with phase transformation and to discuss how to control this process. At first, the nonlinear relationship between the heat flux (q) and the superheat (ΔT), or the boiling curve, is precisely understood, as illustrated in **Figure 1**. In the natural convection flow heat transfer regime, log (q) or logarithm of heat flux increases linearly with the log (ΔT) or logarithm of ΔT. This linear relation between log (q) and log (ΔT) along A – B changes at B. At this point B, the phase transformation occurs from the liquid to its gaseous phase in local. That is, the liquid water locally transforms to the vapor in this local boiling. Starting from B through C to D, the isolated vapor bubbles grow by themselves, gradually agglomerate in themselves on the heating surface, and take off from the heating interface by buoyancy or by forced flow. In this regime, the heat flux significantly increases with increasing the superheat because of the latent heat by boiling, the mass transfer from liquid water to vapor, and the local convection flow.

Those growing vapor bubbles coalesce with each other to form a vapor film when approaching the D point. Once this film locally forms on the heating interface, the heat transfer deteriorates by itself since the thermal conductance significantly reduces in local. The whole interface is covered by this vapor film at D; the heat flux becomes

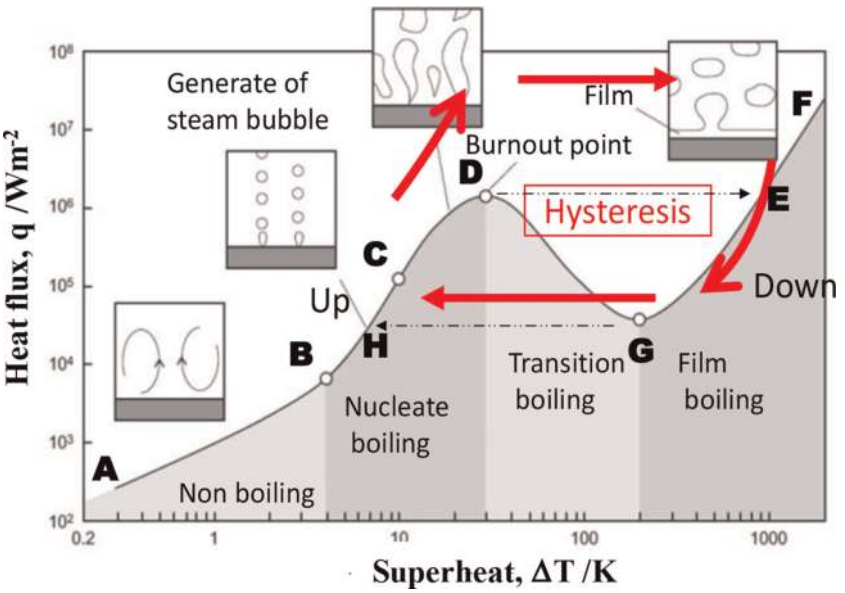

Figure 1.
The boiling curve on the smooth metallic surface [7].

maximum at this point. In the normal heat transfer process, this D point is physically unstable enough to induce the snap-through or the jump of state from the point D to its neighboring stable condition at E even by slightly increasing the heat flux. If the constituent material for heating media had sufficiently high melting temperature not to melt down during this snap-through, the heat transfer process could advance in stable from E to F in **Figure 1**. However, most of metallic heating plates melt down or burn out after this snap-through behavior from D to E.

On the way back by decreasing ΔT from E, this heat transfer process accompanies another nonlinearity. That is, the heat flux decrease from E with decreasing ΔT, and approaches to G where the heat flux minimizes itself under the film boiling regime. At another critical point G, another snap-through takes place from G to H back to the original boiling curve. Every heat exchanging system and device with smooth heating interface has been designed after this boiling curve. The feasible heat flux is limited by the critical heat flux in practice. To be free from this engineering constraint, this relationship must be modified by nontraditional heat transfer process.

To be noticed as the second item, the phase transformation from the liquid water to the vapor bubble commences in local on the heating interface to coolant; each vapor bubble nucleates at the imperfect point on the heating interface. Remember that most of theories on the nonlinear mechanics for heat transfer [7] and buckling mechanics [13] presume the geometric imperfections on the heating interface and on the shell structure, respectively. As summarized in [7], most of classical theories on the boiling heat transfer assumed that a vapor bubble nucleated at the preexisting wedge on the heating interface. Consider that an initial bubble shape is modeled by a half-sphere with its radius of r_c, then, the superheat (ΔT) is inversely proportional to this r_c. When the bubble size is controlled to be small, ΔT increases by itself to start the boiling heat transfer in the early stage of ln (q) – ln (ΔT) relationship in **Figure 1**. In practical situation, few methods were reported to reduce the wedge size, to decrease the wedge depth, to increase the wedge density on the heating interface, to regularize the distribution of wedges, and to control this regularity in the wedge alignment.

The third feature in the boiling process is characterized by the dynamic behavior of vapor bubbles both on the heating interface and in the coolant. After nucleation, one isolated vapor bubble grows, coalesces with each other, and forms a vapor film on the interface. The other bubble takes off from the interface and transports with coolant. The fresh cooling water comes onto the interface to continue this boiling heat transfer process. Unless any bubbles swell on the heated surface, it could be cooled with higher heat flux under constant ΔT. Otherwise, the interface is gradually covered by the vapor bubbles and finally separated from the liquid coolant by the vapor film.

Three engineering items in the above have interaction with each other. The boiling curve in **Figure 1** is governed by the change in vapor bubble morphology. Hence, if the nucleation and growth stages of the vapor bubbles are controlled by micro-texturing the interface, the boiling curve in **Figure 1** is significantly modified in the boiling heat transfer regime. In addition to the studies on controlling the boiling transfer by micro-/nano-texturing [8–12], MEMS (microelectronicmechanical system) technique was utilized to develop the cooling system by impinging the droplets [14] and to investigate the effect of micro-pillared micro-pipe on its thermal performance [15]. Those micro-/nano-texturing methods are useful to demonstrate the improvement of boiling heat transfer in the laboratory scale, but most of them are difficult to be used in the industrial applications. Micro-/nano-textures onto the high

conductive metal members must be essential to find a new way in developing the effective cooling devices with linkage to industries.

Three approaches to form these micro-/nano-textures onto the product surfaces and interfaces were developed feasible to industrial and medical applications. In the plasma-oxidation-assisted printing [16–18], the micro-textures were formed onto the carbon-based materials through oxygen plasma etching. In the plasma-nitriding-assisted printing [19–21], the micro-textures were also formed into the metals and alloys by selectively embedding the nitrogen solute. The extremely short-pulse laser micro-/nano-texturing [22–24] is the third approach to directly imprint the tailored fine textures.

In the first approach, carbon-derivative coatings such as DLC (diamond-Like carbon), CNT (carbon nanotube), graphene sheet, and diamond coatings were processed to yield the carbon-based dies with micro-textures [25–27]. The aspect ratio was predetermined by the coating thickness. In second, the selective nitrogen supersaturation process advanced into the unmasked surfaces and interfaces. The ink-jet printing [19–21], the screen printing [28, 29], and the lithography [30, 31] were utilized as an effective masking techniques. In this case, the aspect ratio of micro-/nano-textures was determined by the nitrided layer thickness up to sub-millimeter thickness. In third, the nano-textured ripples superposed on the tailored micro-textured surface profile by the femtosecond laser processing [32]. In particular, the unidirectional nano-textures were simultaneously formed onto the laser-trimmed tool surface [33, 34]. On the basis of these micro-/nano-texturing methods, the surface-topological design is available to control the heat transfer process with phase transformation on the textured interface [35]. Different from the micro-/nano-texturing by the porous structuring, the particle deposition, and the MEMS techniques in [8–12, 14–15], the regularly or semi-regularly aligned micro-/nano-textures were utilized to discuss the effect of micro-/nano-textures on the aluminum and copper heating devices to the boiling heat transfer in the water vapor system [36, 37].

In the present chapter, two micro-texturing methods are utilized to fabricate the textured aluminum and copper heating units for boiling heat transfer experiments. In the first approach, the plasma-oxidation-assisted plasma printing is used to yield the regular alignment of micro-square pillars on the thick DLC die. This multi-micro-pillared micro-textures on the DLC die are imprinted into the pure aluminum sheet. This concave micro-textured aluminum sheet with regular alignment of micro-cavities is fixed to the copper block to prepare the heating device for heat transfer experiment to describe the vapor bubble nucleation and taking-off behavior. In the presence of micro-cavities on the aluminum interface, the bubble size is reduced by 1/100 or less than that. These super-fine vapor bubbles do not swell on the interface but flow away with the coolant. Due to this change in the vapor-bubble dynamics, the bubble nucleation commences in lower superheat and the heat flux steeply increases with the superheat. In the second approach, the wet plating is utilized to form the acicular Fe–Ni micro-textures onto the oxygen-free pure copper unit for heat transfer experiment to demonstrate the effect of coolant flow velocity or its Reynolds number on the boiling heat transfer. The original boiling curve on the smooth metallic interface is significantly improved by this micro-texturing. The superheat to onset the nucleation of vapor bubbles is reduced by homogeneous and dense generation of bubbles. The heat flux steeply increases with the superheat and exceeds CHF. Through these steps, a physical model is considered to design and fabricate the heat transfer device with $q > q_{cr}$ and $q >> q_{cr}$.

2. Experimental procedure

Two micro-/nano-texturing methods were developed to make concave and convex micro-textures onto the metallic sheets and blocks, respectively. Two experimental setups were prepared to describe the boiling curves, to demonstrate the superiority of micro-textured interface in heat transfer, and to discuss the effect of coolant flow behavior on the boiling heat transfer.

Micro-texturing. The plasma printing method was employed to form the concave micro-textures with regular alignment of square micro-cavities with the specified unit size and pitch onto the pure aluminum sheet. The whole procedure from the micro-texturing design to the CNC imprinting onto the aluminum sheet is depicted in **Figure 2**.

The lithography with ion milling and reactive ion etching was utilized to print the square unit cell pattern with the size of 3.5 μm x 3.5 μm and the pitch of 5 μm onto the DLC-coated AISI420 punch with the coating thickness of 15 μm. Then, the platinum deposit on the nano-carbon film was left as a unit cell. The controlled oxygen plasma etching system was utilized to chemically remove the unmasked DLC regions and to fabricate the micro-pillared DLC coating punch. This punch was inserted into a die set for CNC imprinting of micro-pillar textures into the aluminum sheet. The original two-dimensional micro-texture pattern transformed to the three-dimensional regular alignment of micro-cavities on the aluminum sheet. The wet plating was employed to directly form the convex micro-textures onto the oxygen-free copper specimen with use of the nickel and iron-ionized solution. Each unit cell of acicular Fe-Ni crystals nucleated and grew on the substrate surface as depicted in **Figure 3**. Every acicular unit cell aligned with each other in semi-regular on the substrate. Its root size and height were completely determined by the wet plating conditions including the

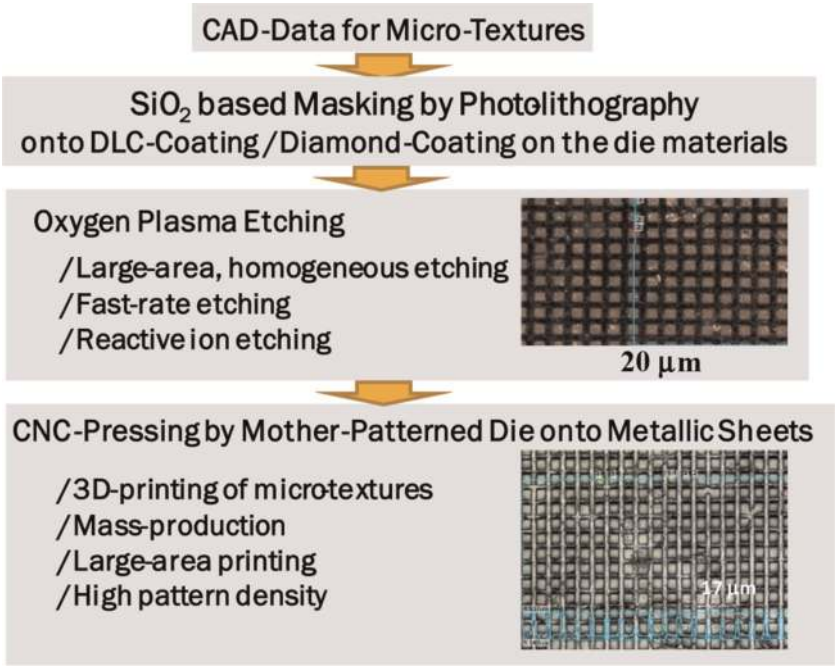

Figure 2.
A plasma printing procedure from the CAD (computer-aided design) of micro-textures through the fabrication of micro-textured DLC die to the CNC (computer numerical control) – Imprinting to metallic sheet.

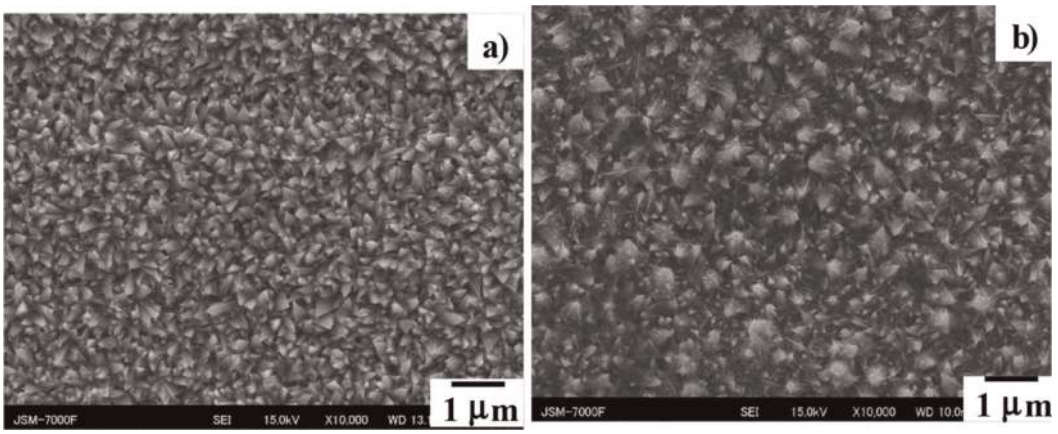

Figure 3.
Nucleation and growth of Fe-Ni acicular unit cells on the substrate during the wet plating. a) τ = 210 s, and b) τ = 630 s.

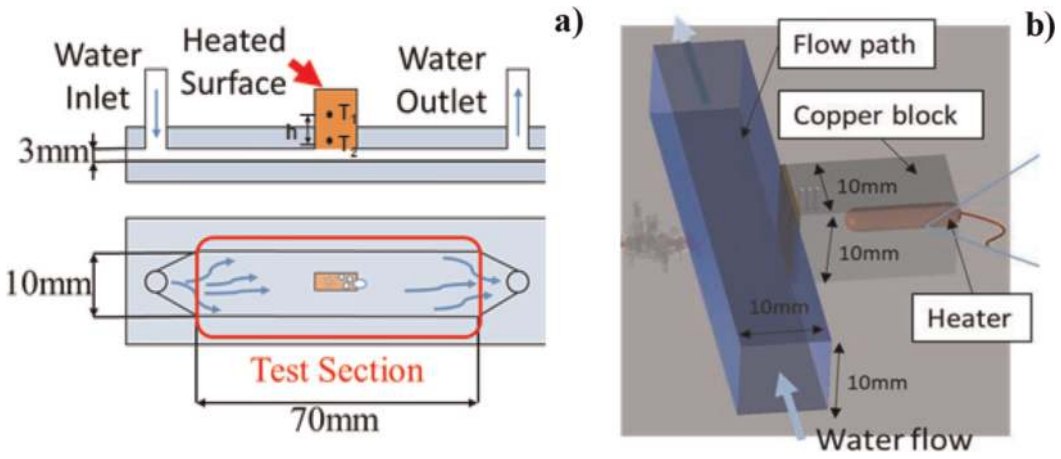

Figure 4.
The boiling heat transfer experimental test sections. a) Narrow, lateral channel section to observe the vapor bubble nucleation and taking-off phenomena with the measurement, and b) square, longitudinal channel section to investigate the effect of coolant flow on the boiling heat transfer.

duration (τ). In **Figure 3a**, when τ is 210 s, the root size (B) of acicular micro-texturing unit cell ranged from 0.1 to 0.4 μm, and its height (H) was 0.5 μm in average. This tiny unit cell significantly grew as compared between **Figure 3a** and **b**. When τ = 730 s, B ranged from 0.2 to 0.7 μm, and H ∼ 1 μm.

Heat-transfer test-sections. In the following experiments, two test sections were used to describe the vapor bubble nucleation and taking-off and to investigate the micro-texturing effect on the boiling heat transfer process. In the first setup, the coolant channel with the length of 70 mm is laterally placed so that the subcooled water is heated by the copper block as depicted in **Figure 4a**. Pure aluminum devices with and without micro-textures were joined to the top of this block. The heat flux (q) through these devices was measured by the difference of temperature histories in the block. High-speed video camera was also utilized to visualize the vapor bubble nucleation and its taking-off from the aluminum devices.

Figure 4b shows another setup to measure the heat transfer characteristics with the use of the heating copper block. The micro-textures were directly yielded onto this

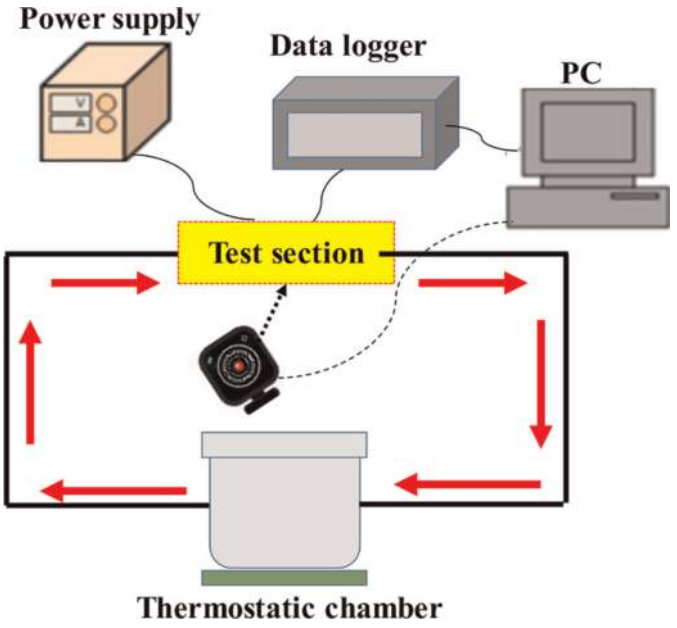

Figure 5.
Experimental setup for measurement and observation of the boiling heat transfer in the test-section.

block. The water channel stood in vertical to control the flow velocity and to investigate the effect of forced coolant velocity on the heat transfer. The heat flux was measured in the similar manner to the setup in **Figure 4a**.

These test sections were respectively set up into the experimental system including the power controllers and the monitoring apparatus, as illustrated in **Figure 5**. The superheat was directly controlled by the applied voltage in the power supply. The thermostatic chamber was utilized to keep the subcooled water temperature by 30 K and to control the coolant velocity. The measured temperature histories were monitored by using three thermocouples, which were embedded into the copper heating block. The surface temperature on the interface was estimated by directly extrapolating the measured temperature depth profile in the block. The heat flux was also calculated from this profile by using the Fourier's law, which was represented by

$$q = -\kappa(\delta T/\delta X), \tag{1}$$

where κ was the thermal conductivity of copper, δT was the difference between two measured temperatures away from each other by the distance of δX. The whole data were transferred and accumulated in PC.

The digital video imaging unit was utilized to record the time history of the boiling and cooling behavior in the inside of channels through the transparent window. The vapor bubble nucleation and growth process were directly monitored to describe the effect of coolant velocity on the boiling behavior.

3. Experimental results

Regular alignment of micro-cavities onto aluminum sheet. Two-dimensional micro-pattern was printed by the lithography onto the DLC film coated on the AISI420 substrate. A square dot with 3.5 μm x 3.5 μm was aligned with the pitch of

5 μm on this DLC coating die. The unprinted DLC films were chemically etched out by using the high-density plasma oxidation system. Through this plasma oxygen etching for 5 ks, a DLC micro-pillared punch array was fabricated by selectively removing the unprinted mesh-lines of DLC films with their width of 1.5 μm. As depicted in **Figure 6a**, the arrayed DLC-punch by plasma oxygen etching had a square micro-pillar head with its area of 3.5 μm x 3.5 μm and its height of 8 μm. The depth profile of DLC punch array was measured by the laser surface profilometer and supposed in **Figure 6a**. DLC micro-pillars with the same head size were regularly aligned with the pitch of 5 μm by the plasma oxidation etching. This regular alignment of micro-pillars onto the DLC-punch assures the regular duplication of micro-textures in inverse to micro-pillars into the metallic sheets or plates by the precise stamping with the use of this DLC-punch.

CNC stamping system was utilized for this imprinting of DLC micro-pillar array into the as-rolled pure aluminum sheet with the thickness of 0.2 mm. As shown in **Figure 6b**, the micro-cavity array was imprinted onto the aluminum sheet surface by indentation of the DLC micro-pillar array in **Figure 6a**. Through this indentation of DLC-punch, the pure aluminum work was extruded in backward into the clearance with the width of 1.5 μm between adjacent DLC pillars. The thin walls of each aluminum micro-cavity were formed to have the thickness of 1.5 μm. That is, each DLC pillar with its head size of 3.5 μm x 3.5 μm was simultaneously indented to shape a bottom of a micro-cavity with the size of 3.5 μm x 3.5 μm. Four clearances surrounding each DLC micro-pillar became four micro-cavity side walls with the width of 1.5 μm and the height of 5 μm. Then, the micro-pillar alignment on the DLC-punch was duplicated to the aluminum sheet as a regular micro-cavity array with its unit cell of 3.5 μm x 3.5 μm x 5 μm and the pitch of 5 μm. This imprinting process incrementally advanced by stamping the DLC-coated AISI420 punch with the head size of 80 mm x 10 mm into the pure aluminum sheet. Each stamped aluminum sheet segment had 3.2 x 10^7 micro-cavities on its area of 80 mm x 10 mm. Then, the density of micro-cavities reached 4 x 10^4/mm^2.

Figure 7 compares the aluminum sheets without and with the micro-cavity textures. The static contact angle of pure water onto the aluminum sheets increased from 92° for smooth surface to 110° by this micro-texturing.

Bubble heat transfer on the concave micro-textured interface. The pure aluminum sheet segment with micro-cavity alignment and the bare aluminum one were

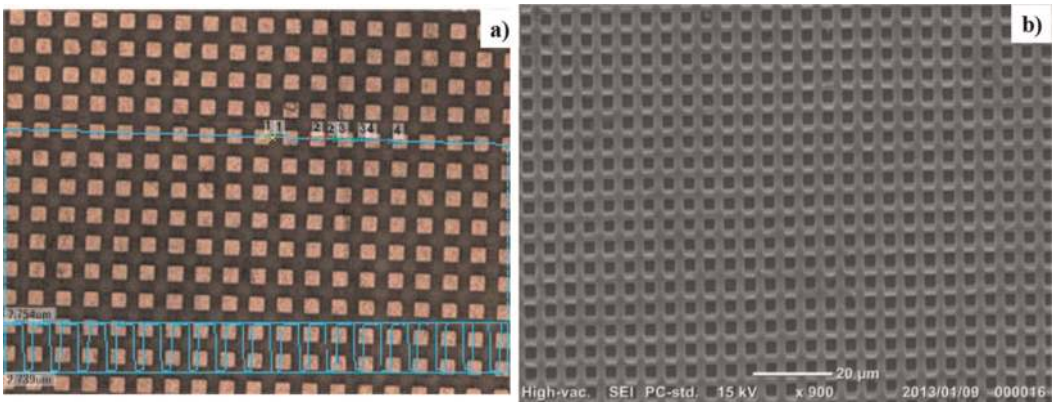

Figure 6.
Comparison of the micro-pillared DLC die surface with the CNC-imprinted aluminum sheet. a) DLC micro-pillar alignment on the die, and b) micro-cavity alignment on the aluminum sheet.

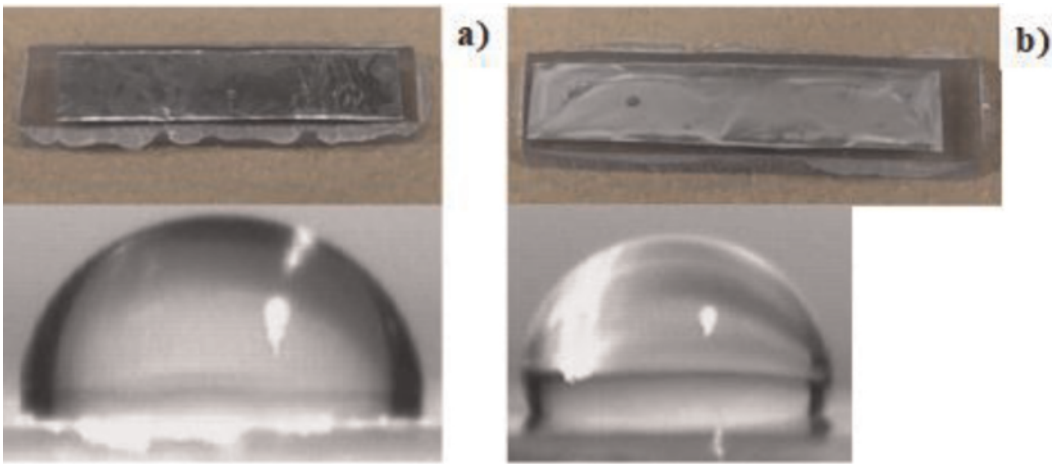

Figure 7.
Comparison of aluminum sheet without and with micro-textures. a) Aluminum sheet without micro-textures (contact angle of pure water on its surface (θ) is 92°), and b) aluminum sheet with micro-textures (θ = 110°).

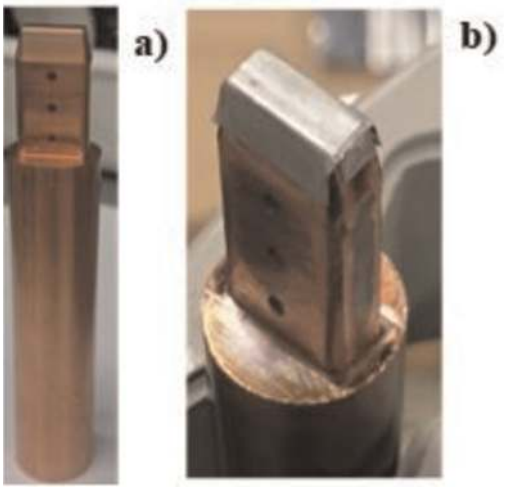

Figure 8.
*A heating block in the setup in **Figure 4a**. a) a bare copper heating block, and b) heating block with the joined aluminum sheets in **Figure 6** by using the nanoparticle silver paste.*

respectively joined to the copper block by using the nanoparticle silver paste. **Figure 8** compares the heating copper block before and after joining the aluminum sheet segment. Except for the thermal gap in conductance by this silver paste, this heating block was suitable to experimental analysis on the effect of micro-textured metallic sheet on the boiling heat transfer. This heating block was fixed into the test section in **Figure 4a**. In this setup, the phase transformation from the liquid water to the vapor bubble took place on the surface of aluminum device with and without the micro-cavity textures.

Figure 9 depicts the nucleation and growth stage of vapor bubbles on the aluminum sheet without and with micro-cavities. As shown in **Figure 9a**, when the micro-textures were absent on the aluminum sheet, large vapor bubbles only nucleated and swelled on the interface and grew by themselves. No taking-off of bubbles was observed by the video imaging.

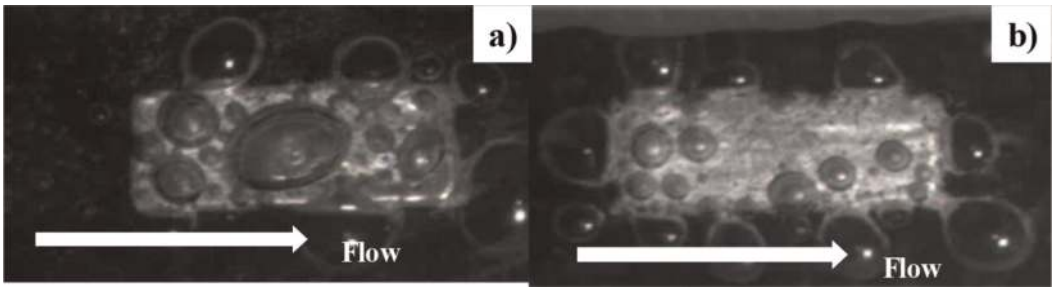

Figure 9.
A bubble nucleation on the aluminum sheet a) without the micro-textures and b) with the micro-texture.

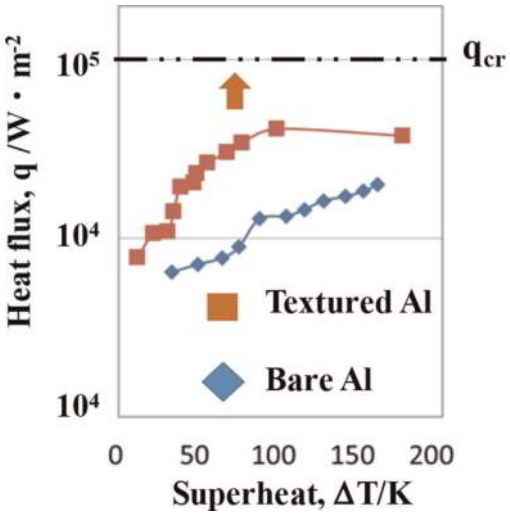

Figure 10.
Comparison of the boiling curves in the heat transfer through the aluminum sheets with and without the micro-textures.

On the other hand, as depicted in **Figure 9b**, only fine bubbles with the average size of 5–10 μm nucleated on the interface without significant growth. Most of them flew away together with the coolant and the medium-sized bubbles. As compared between **Figure 9a** and **b**, the heating interface with micro-textures was cleared by this flow-away of fine vapor bubbles. This easiness of vapor bubble taking-off from the heating interface enabled new liquid coolant to directly come onto the interface for further heat transfer. Owing to this micro-texturing effect on the bubble nucleation and growth mechanism, the heat transfer on the aluminum interface between the heating block and the coolant was much improved in the presence of micro-textures.

Figure 10 depicts the relationship between the measured heat flux q and the superheat ΔT with and without micro-textures. When using the bare aluminum interface, the heat flux gradually increased with ΔT and the onset superheat to nucleate the boiling was retarded in correspondence to the normal heat transfer mechanism in **Figure 1**. On the other hand, in the presence of micro-textures on the aluminum interface, the heat flux steeply increased with ΔT at the beginning of superheating. The onset of superheat for bubble nucleation started earlier than the normal boiling nucleation. Although this increasing heat flux was suppressed around ΔT = 60 K due to the insufficient coolant flow volume, the micro-textures enhanced the increase of heat flux with ΔT so that q approaches to the critical heat flux, q_{cr}.

This heat transfer through the micro-cavity arrayed aluminum device teaches:

1. the bubble size is reduced by decreasing the wedge size,

2. the onset superheat of ΔT_{onset} to nucleate a mass of bubbles is also reduced, and

3. the heat flux q increases steeply toward the critical heat flux, q_{cr}.

After the classical theory, the effect of the wedge size on the heat transfer is considered by

$$\Delta T \sim 2\sigma T_{sat}/[\rho_v \bullet \Delta h_v \bullet r_c \bullet (1 - r_c/\delta)] \quad (2)$$

In this relation, σ denotes the thermal conductivity, T_{sat} is the saturated temperature, ρ_v is the mass density of coolant, Δh_v is the latent heat, r_c is the radius of wedge, and δ is the thermal boundary layer thickness. From Eq. (2), the superheat increases by decreasing r_c. On the other hand, ΔT_{onset} decreased with decreasing the micro-cavity size in **Figure 8**. This contradiction between the classical model and the experimental results is attributed to vapor bubbling mechanism on the interfaces without and with the regular micro-cavity alignment.

The classical knowledge by Eq. (2) presumes that each vapor bubble nucleates at the preexisting wedge on the flat interface through the phase transformation of liquid coolant in local. This nucleation and growth process advances independently in each bubble, which is isolated from the neighboring bubbles. In this low bubble density nucleation and growth process, higher superheat is needed to stimulate the nucleation and growth step for each bubble till it takes off from the wedge. In the heat transfer across the micro-textured interface, many bubbles nucleate simultaneously at the regularly aligned wedges with the specified distance between adjacent wedges. Under this high bubble density nucleation from regularly distancing wedges by 5 μm in **Figure 6b**, lower superheat was enough to nucleate a fine bubble in the surrounding coolant flows. **Figure 9b** reveals that a mass of fine bubbles easily moves with the coolant flow and that the interface is cooled down to restart the bubble-nucleation stage under the fresh coolant. That is, the generated bubble size is much small enough to drive the routine of bubble nucleation, growth, and taking-off promptly and repeatedly. This tiny bubbling routine on the heating interface with regularly aligned concave micro-texture modifies the original boiling heat transfer mechanism in **Figure 1** and pushes up the heat flux even at the lower superheat.

Two engineering items are considered to further control the boiling heat transfer by micro-texturing. In the first item, the micro-textured interface property is taken into account together with the regular alignment of micro-cavities or wedges in **Figure 7b**.

Since the metal surface is usually hydrophilic with the static contact angle of 60°–70°, this surface condition is controlled by micro-/nano-texturing to be more hydrophilic or to be hydrophobic, as an engineering policy. In second item, the coolant design is surveyed to improve the q – ΔT relationship or the boiling curve. Among several parameters, the coolant flow velocity is employed as an important item. After the classical treatise on the boiling heat transfer [7], its mechanism was considered to be invariant to the coolant flow velocity. There is a possibility to improve the q – ΔT relationship with increasing the flow velocity or the Reynolds number of coolant on the micro-textured interface.

Semi-regular alignment of micro-acicular textures onto copper. The wet plating process was employed to build up the acicular iron-nickel (Fe–Ni) alloy micro-textures directly onto the copper heating block surface. The acicular Fe–Ni pyramids nucleated and grew onto the copper surface with increasing the duration in the wet plating, as stated before. In particular, as depicted in **Figure 11a**, the root size and height of acicular pyramids were controlled by the wet-plating conditions.

Since no pastes were used in this micro-texturing, no thermal gap conductance was present between the micro-textured layer and the heating copper block. As shown in **Figure 11b**, this acicular Fe–Ni layer was thermally well-contact to the top surface of copper heating block. In the previous experiment, the micro-textured aluminum sheet was joined to the copper block by using the solder paste. Then, the measured q – ΔT relationship was biased by its thermal gap conductance. In this second experimental setup, the micro-textured layer was directly deposited onto the copper heating block head surface without the use of paste. The heat flux in the copper block was directly conducted to the wet-plated Fe–Ni layer without loss of thermal conductance. The acicular micro-textures influenced on the surface property and on the vapor bubble nucleation and growth during the boiling process.

Two Fe–Ni acicular layers were formed onto the copper block by varying their unit cell size to understand the micro-texture size effect on the boiling heat transfer mechanism. The microstructure of the first Fe–Ni micro-textured film (specimen-1) is shown in **Figure 12a**. Three-dimensional profilometer was utilized to define the average height (H) of acicular unit cell, the average spacing (D) between adjacent unit cells, and the aspect ratio (H/B) of H to the average bottom size (B) of unit cells. This specimen-1 has H = 1.6 μm, D = 3.9 μm, and H/B = 0.42. As depicted in **Figure 12b**, this textured surface becomes hydrophilic with the contact angle of 20–30°. A bare copper block is also used as a reference to compare the q –ΔT relationship with two micro-textured specimens. The mechanically ground copper interface has the average roughness of Ra = 0.6 μm and Rz = 1.2 μm. Due to this surface roughness, the contact angle reaches 100–110°; the copper interface is hydrophobic.

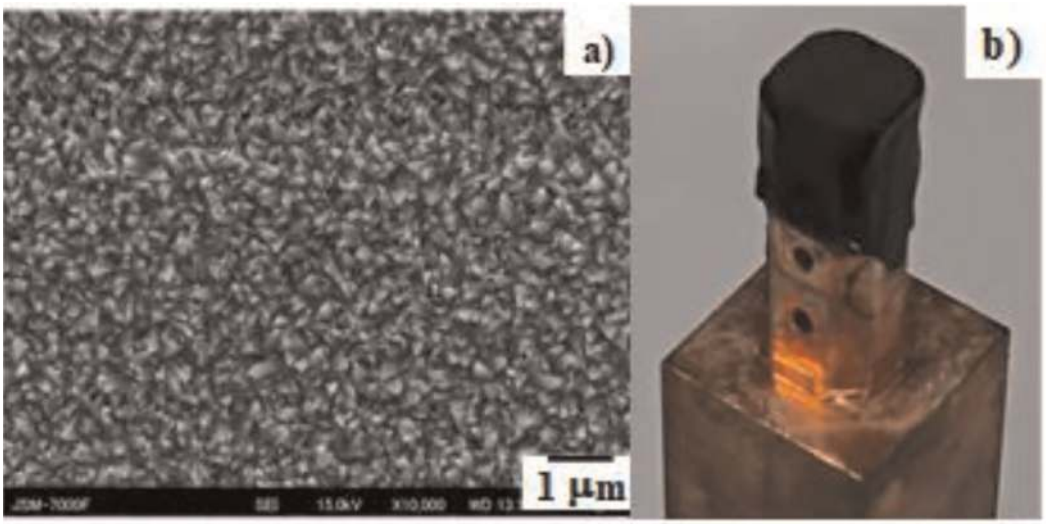

Figure 11.
An acicular Fe–Ni alloy film, wet-plated onto the copper heating block. a) SEM image on the wet-plated Fe – Ni alloy film, and b) copper heating block with the Fe–Ni layer on the top of block.

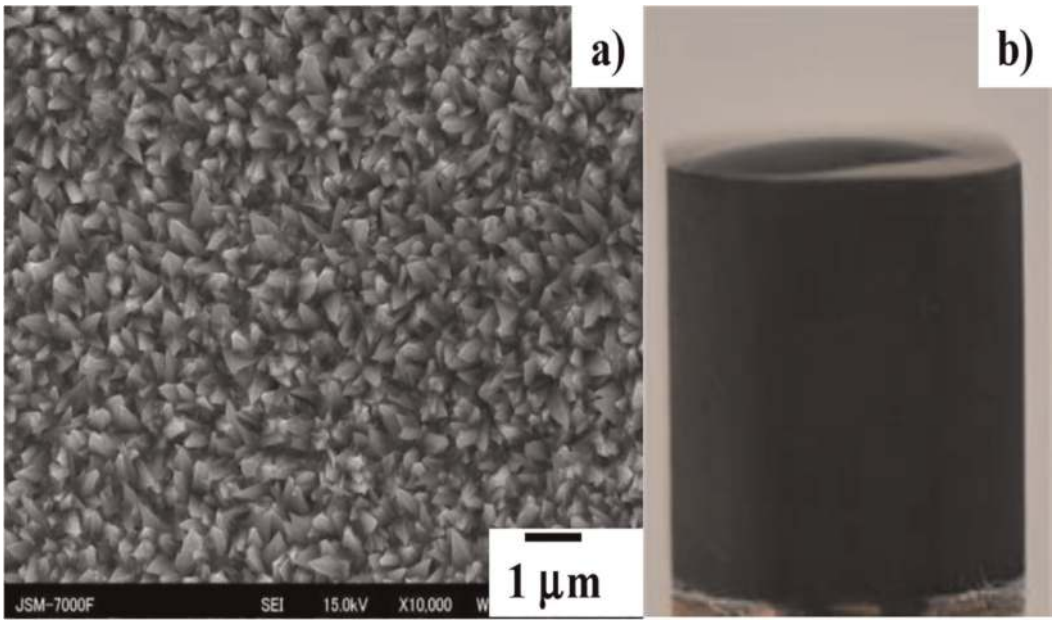

Figure 12.
The first Fe–Ni micro-textured heating block specimen-1. a) Its microstructure in the plain view, and b) its wettability.

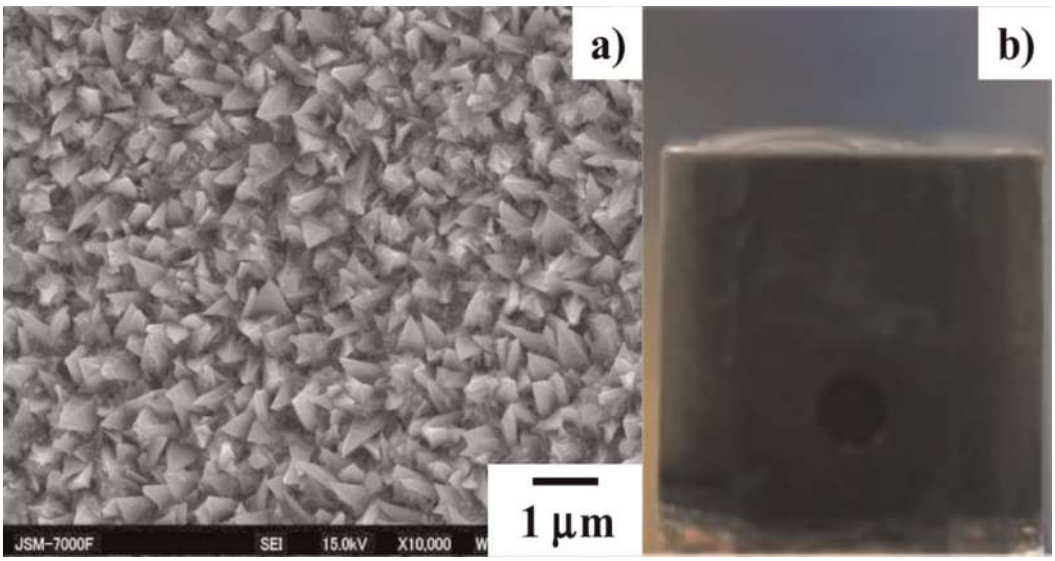

Figure 13.
The second Fe–Ni micro-textured heating block specimen-2. a) Its microstructure in the plain view, and b) its wettability.

Remembering that a smooth metallic surface is usually hydrophilic with the contact angle of 40–70°, this high contact angle implies that original roughness of copper block surface influences the measured boiling curve. In particular, this micro-textured surface of specimen-1 has nearly the same geometric features as the bare copper surface.

The second specimen or specimen-2 was prepared by the wet plating with longer duration. **Figure 13a** shows the SEM image of the Fe–Ni acicular microstructures on the copper block. The micro-textures in **Figure 13a** have a self-similar morphology to the specimen-1 in **Figure 12a**. This Fe–Ni acicular unit cell has H = 4.8 μm, D = 2.2 μm,

and H/B = 0.46. After the wettability testing, this specimen is also hydrophilic with the same contact angle.

By using two specimens in the above, the boiling heat transfer experiments in **Figure 3b** are performed to investigate the effect of the acicular micro-textures on the q – ΔT relationship and the heat transfer mechanism.

Boiling heat transfer on the convex micro-textured interface. Two types of experiments are performed in the following. In the former experiment, the acicular micro-texturing effect on the heat transfer is investigated. In the latter, the effect of coolant velocity or Reynolds number (Re) to the heat transfer mechanism is precisely discussed. In the first experiment, the coolant velocity was held constant by V = 1.9 m/s or Re = 460. The coolant was completely degassed and its temperature was also controlled to be 347 K or subcooled by 30 K. The copper block was gradually heated by increasing the applied voltage in every 10 V.

In correspondence to the boiling curve in **Figure 1**, q increases gradually with increasing ΔT in case of copper block without the micro-textures. When using the specimen-2 with its microstructure in **Figure 14**, the heat flux rapidly increases with ΔT after the superheat of ΔT = 2 K, and approaches the critical heat flux, q_{cr} at ΔT = 17 K. Remember that q = 0.9 x 10^6 W/m^2 at ΔT = 17 K when using the copper block without the micro-textures. The heat flux becomes two and a half times higher at the same superheat of 17 K by using this hydrophilic micro-texture.

On the other hand, in case of the specimen-1 in **Figure 12**, its q – ΔT relationship becomes nearly the same as q – ΔT for non-textured specimen. This is because the micro-textured interface of specimen-1 has nearly the same topological aspects as the bare copper interface. The difference between two specimens implies that the boiling heat transfer behavior becomes sensitive to the acicular micro-texture morphology under the laminar coolant flow. To be noticed, q_{cr} on the micro-textured surfaces seems to be always more than q_{cr} on the smooth surface.

In the second experiment, the coolant flow velocity was increased to change the laminar flow to the turbulent flow and to investigate the sensitivity of boiling heat transfer mechanism to the flow pattern change. The specimen-1 was employed in this experiment, while the bare copper specimen was also used as a reference. **Figure 15** compares the variation of q – ΔT curves with increasing the Re between the specimen-1 and the normal copper block without micro-textures.

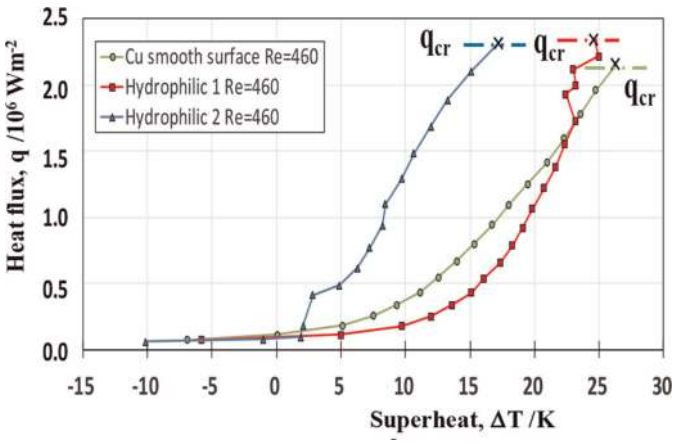

Figure 14.
Comparison of the boiling curves under the laminar flow condition among the copper smooth surface and two micro-textured copper surfaces.

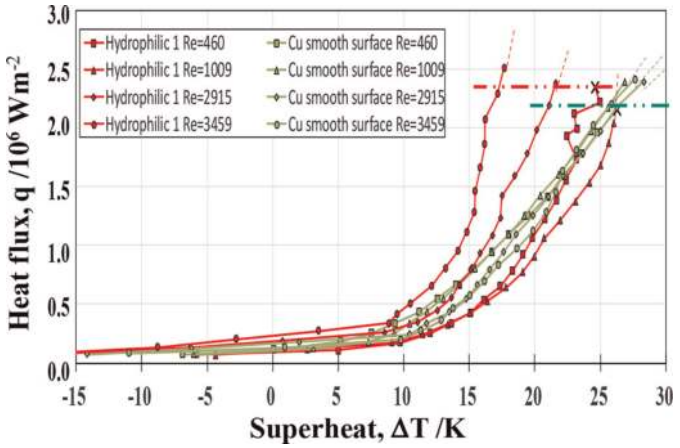

Figure 15.
Q – ΔT relationships for normal copper block without micro-textures and for the specimen-1 with increasing Re.

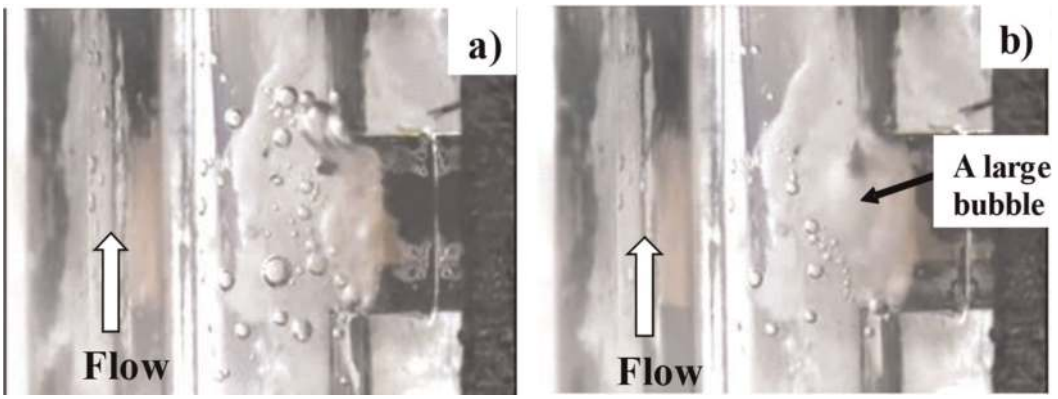

Figure 16.
High-speed camera flame on the nucleation boiling process on the bare copper block head without micro-textures in the coolant channel at Re = 3459 with increasing the applied power (P) for heating. a) P = 110 W, and b) P = 180 W.

When using the bare copper heating block, four measured q – ΔT relationships in **Figure 15** are nearly the same among them and insensitive to the coolant velocity even by increasing Re from 460 to 3459, or by changing the laminar flow to the turbulent one. This insensitivity of boiling heat transfer process to the Reynolds number was just stated in the classical treatise [7]. The coolant flow pattern has nothing to do with the boiling heat transfer process or the bubble nucleation and growth process in the classical common knowledge. This is because each wedge on the bare copper is isolated from each other and a bubble nucleates and grows mainly in the function of superheat.

In case of the micro-textured specimen-1, the onset of superheat to nucleate the bubbles is reduced and the gradient of dq/d(ΔT) becomes steeper with increasing Re. CHF also seems to increase with increasing Re. This enhancement of q – ΔT relationship with Re implies that a mass of vapor bubbles is transported by the coolant flow and that the fresh coolant comes onto the heating interface.

The video imaging often helps to describe the boiling behavior with increasing the electrical power (P). In the following, an overall boiling and flow behavior is observed during the heat transfer experiment by using two snap-shots in the video

imaging. **Figure 16** depicts the boiling and flow processes in the coolant channel under Re = 3459. When P = 110 W, the coolant was uniformly boiled in down- and upper streams, surrounding the heating copper block head as shown in **Figure 16a**. The small-sized bubbles were seen in this boiled coolant, but the boiled coolant region widened symmetrically in both streams of coolant. A fresh coolant did not approach the heating copper block head for further forced cooling. When increasing the power to P = 180 W, the boiled coolant pattern in **Figure 16b** was nearly the same as seen in **Figure 16a**. The boiling behavior did not change itself by increasing the applied power to the heating unit. Larger bubbles were seen in **Figure 16b**; the bubbles nucleated and easily agglomerated themselves to form a larger bubble. This appearance of large bubbles teaches a signal of risk where these large bubbles promptly coalescence to a film at the vicinity of interface, and the nucleate boiling mode changes to the film boiling mode. That is, the nucleate boiling behavior in **Figure 16b** continues by itself till the burn-out point when the heat flux approaches the critical one.

The difference of q–ΔT relationship with and without micro-textures in **Figure 15** predicts that the nucleation boiling process in **Figure 16** with increasing the power changes itself by the micro-texturing on the heating copper block head.

In using the same experimental setup, the nucleation boiling behavior on the micro-textured copper block is analyzed by high-speed camera. When P = 110 W, the boiling coolant region was seen only in the downstream and became narrow near the micro-textured interface between the heating copper block and coolant in **Figure 17a**. When P = 180 W, the bubbled coolant flew away in the downstream together with the main coolant as seen in **Figure 17b**. To be noticed, a single-phase or liquid-phase coolant entered into the channel inlet, mixed with the two-phase, turbulent flow from the interface, and flew away from the channel outlet in **Figure 4b**. This observation on the flow pattern at Re = 3459 reveals that the coolant flow has a significant interaction with the boiling heat transfer on the micro-textured interface. Two-phase mass with fine bubbles moves away from the vicinity of interface to the downstream of coolant. The micro-textured interface is cooled down by a new coolant from the upper stream. The mixing process of two flows and the mass transfer of fine bubbles to coolant flow work independently to sustain the higher heat transfer through the micro-textured interface. This results in the steep increase of heat flux to CHF and above CHF even at lower superheat.

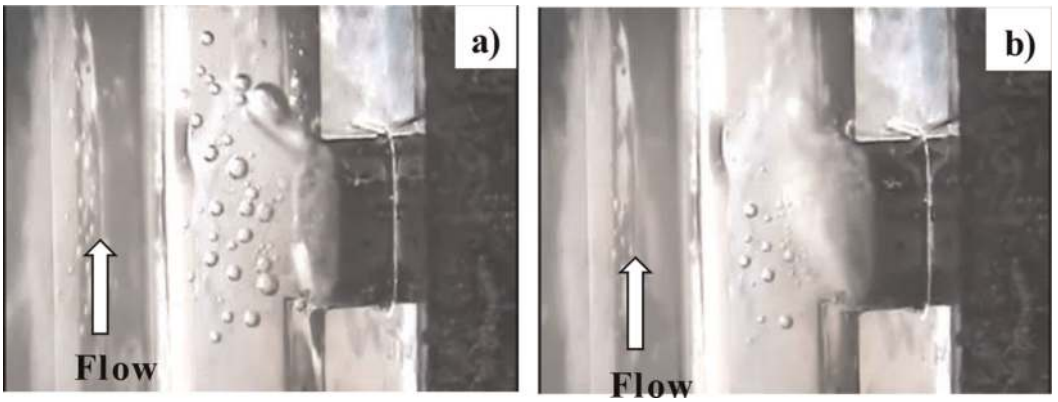

Figure 17.
High-speed camera flame on the nucleation boiling process on the micro-textured copper block head in the coolant channel at Re = 3459 with increasing the applied power (P) for heating. a) P = 110 W, and b) P = 180 W.

Micro-texturing effect on coolant flow and heat transfer. A micro-texture on the interface has a possibility to influence both on the flow behavior and the heat transfer. Various studies have been reported on the effect of micro-texture to the coolant turbulent flow in the literature [38]. After those results, the turbulent flow behavior at the vicinity of the channel wall is affected by the viscous effect. In this viscous sub-layer, its friction velocity u* is estimated by the following equation with the Blasius equation for friction factor λ,

$$u^* = \sqrt{\frac{t_0}{\rho}}, t_0 = \frac{1}{8}\lambda\rho u^2, \lambda = 0.3164\, Re^{-\frac{1}{4}}, \tag{3}$$

From this friction velocity, let us calculate the wall coordinate (y+) at the height of the micro-texture. In the above experiment, Re = 3459; then, u* = 0.0103 m/s. Since the height of micro-texture is k_s = 2.2 μm or 2.2 x 10^{-6} m, and the kinetic viscosity of coolant is ν = 4.13 x 10^{-7} m^2/s, y + = u* k_s/ν = 0.04. This y + is much lower than the critical number of ~5. The surface angulation by this micro-texturing is identified to be included into the viscous sub-layer. That is, this microstructure has nothing to do with the coolant turbulent flow, and it can be regarded as a hydraulically smooth surface.

Next let us consider the micro-texturing effect on the heat transfer coefficient. The turbulent flow heat transfer on the flat interface without the micro-textures is described by the Nusselt number (Nu). After [39], this Nu is expressed by the function of the Reynolds number and the Prandle number (Pr) in the following:

$$\mathrm{Nu} = 0.023\ \mathrm{Re}^{0.8}\mathrm{Pr}^{0.4} \tag{4}$$

Since the heat transfer coefficient (h) is proportional to Nu, h ~ $Re^{0.8}$ on the flat interface. On the other hand, the measured h (= q/ (T_w – T_L)) on the micro-textured interface is estimated from **Figure 15** to be

$$\mathrm{h} \sim \mathrm{Re}^{\mathrm{n}} \tag{5}$$

Here, n is a power exponent, which is given by n = 2.71 at ΔT = 9 K, n = 2.79 at ΔT = 15 K, and n = 3.31 at ΔT = 17 K. This result with n > 0.8 proves that the boiling heat transfer is much enhanced by the coolant turbulent flow on the micro-textured interface. Remembering that micro-textures have no influence on the turbulent flow profile, this enhancement is induced by the vapor-bubble transportation with high coolant flow velocity even in the viscous sub-layer.

4. Discussion

Boiling curves on the micro-textured interface. The micro-/nano-texturing onto the heating device surface has a significant influence on the boiling heat transfer. First, the heat flux to superheat relationship in **Figure 1** is controlled by the micro-/nano-texturing. The superheat to start the nucleation of vapor bubbles is much reduced, the heat flux gradient by ΔT or the heat penetration factor (K_q) becomes steep along B – C – D curve, and the heat flux can exceed the critical heat flux (CHF).

In second, the classical model on the nucleation and growth of vapor bubbles must be exchanged with a new physical model, where superfine vapor bubbles nucleate on the micro-/nano-textured interface and flow away with coolant flow. In particular, the

nucleation and growth of vapor bubbles are dependent on the local geometric topology of micro-/nano-textures. The bubble density, nucleating on the textured interface, much increases even in the early stage on B – C regime.

In third, higher heat flux is attained even at lower superheat with increasing the coolant flow velocity or its Reynold number. In the absence of textures on the heating interface, the boiling heat transfer has nothing to do with the flow velocity change from the laminar flow to the turbulent flow. This is just corresponding to the classical theory in [7]. In the presence of micro-textures, most of vapor bubbles densely nucleate and easily take off from the heating interface at the early stage of superheating. Since the local mass in two phase with lots of fine bubbles moves away with main turbulent flow of coolant, higher heat flux is attained even at the lower superheat.

Standing on these engineering items, a new boiling curve is proposed for the boiling heat transfer process through the micro-/nano-textured heating surface.

The heat flux to superheat relationship on the micro-textured interface is schematically depicted in **Figure 18** with comparison to the boiling curve on the flat interface. The vapor nucleation starts at B′ or at $\Delta T = \Delta T_i$; the point B′ becomes a turning point from the natural or forced convection heat transfer along A' – B′ to the nucleation boiling process. This intrinsic superheat (ΔT_i) is determined by the minimum thermal conductance of the micro-/nano-textured layer; this ΔT_i is much smaller than ΔT in **Figure 1**. Along the line B′ to C′, the heat flux increases with the steep gradient of K_q even under the laminar coolant flow. This heat penetration rate, K_q, is strongly dependent on the geometric topology of micro-/nano-textured layer. In case of the present acicular micro-textures, their unit cell size, height, aspect ratio, and their alignment have essential influence on K_q. At C′, the heat transfer process is enhanced by the coolant flow pattern change from the laminar flow to the forced turbulent flow. Under the continuous mass transfer of two-phase coolant with dense fine bubbles to the main flow, the heat flux exceeds the CHF and increases monotonously with ΔT above CHF.

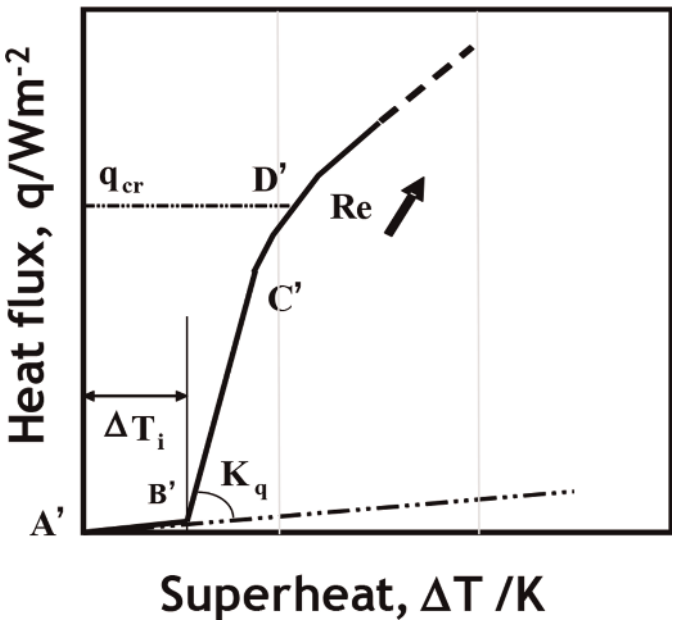

Figure 18.
A new boiling curve for boiling heat transfer on the micro-textured interface between the coolant and the heating solid.

From **Figures 10** and **15**, this ΔT_i was estimated to be less than 10 K and $K_q \sim 0.2$ x 10^6 W/(m^2•K). The onset temperature of bubble nucleation, ΔT_{onset} reduced to ΔT_i in these Figures. The bubble nucleation at the single wedge on the flat surface is retarded so that $\Delta T_{onset} > \Delta T_i$. On the other hand, the phase transformation to vapor bubbles commences at every spot near the aligned micro-textures at the same time. That is, the micro-/nano-texturing onto the heating surface stimulates the onset of bubble nucleation at the network of micro-cavities in **Figure 10** and at the micro-pillars in **Figure 15**. This difference of onset superheat reveals that the mode change from the convection heat transfer process to the boiling heat transfer process is triggered in the very early stage of superheat by the simultaneous nucleation of fine bubbles in mass.

The least onset superheat of ΔT_i is needed for thermal conductance of micro-/nano-textured layer. In case of the heat transfer on the flat interface, the difference of ($\Delta T_{onset} - \Delta T_i$) is needed to trigger the phase transformation to vapor at each isolated wedge on the interface. This retardation is reduced, or, $\Delta T_{onset} \rightarrow \Delta T_i$ by simultaneous nucleation of fine vapor bubbles due to the micro-/nano-texturing. The simultaneous nucleation reflects on the increase of bubble density even at lower superheat.

The steep branch at B′ with high gradient of K_q in **Figure 18**, implies that the fine bubbles nucleating at the micro-textures easily take off from the heating interface to the main stream of coolant. Until this nucleation and taking-off continues even in increasing the superheat, the heat flux increases even under the laminar coolant flow. After the nucleation mode changes to the growth mode of bubbles, the increase of heat flux by ΔT becomes redundant and slow. In particular, $q/\Delta T$ in the forced turbulent coolant flow regime is still large enough to sustain the flow interaction between the generated two-phase local flow and the main forced coolant flow.

Bubble density nucleating on the micro-textured interface. Nucleation of super-fine vapor bubbles and their taking-off with coolant is essential to start the boiling heat transfer at lower superheat and to sustain high heat flux condition. The unit-cell size and its pitch play an important role to reduce the vapor-bubble size and to increase the bubble density. Through the image processing of frame pictures in **Figures 9b, 17a**, and **b**, the vapor-bubble size was still larger than the unit-cell size; e.g., the unit-cavity size of micro-textures was 3.5 μm x 3.5 μm but the bubble size was larger than 10 μm. In other words, the local phase transformation process is redundant to nucleate the vapor bubble at the selected unit cell among many nucleation sites. This low bubble density suppresses the actual heat flux to be slightly higher than CHF.

Micro-/nano-texture design for enhancement of heat transfer. In the present study, two types of micro-textures were employed to investigate the interface conditions on the boiling transfer process; e.g., the concave micro-textures with hydrophobicity in **Figure 7**, and the convex micro-textures with hydrophilicity in **Figures 12** and **13**. The controllability of wettability by micro-texturing has been intensely discussed through previous studies in the literature [32]. Let us describe the effect of surface properties on the micro-textured interface to the heat transfer. High surface energy surface is preferable to cover the whole surface by coolant liquid and to easily release the nucleating vapor bubbles. That is, the micro- and nano-textures might well be redesigned to consider their multiple functions in the boiling heat transfer mechanism. The measured $q - \Delta T$ relationships in **Figures 10** and **15** suggest that the interfacial condition seems to have little influence on the boiling heat transfer process. Other micro-/nano-texturing features might have more importance on the improvement of boiling heat transfer process; e.g., the multidimensional texturing with self-similarity, the super-hydrophilic texturing with high aspect ratio and the super-hydrophobic texturing with higher spatial frequency ratio.

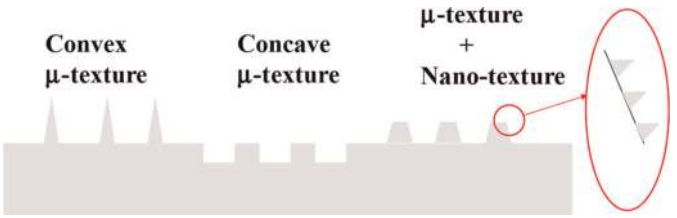

Figure 19.
Feasible micro-/nano-texturing onto the heating interface.

As illustrated in **Figure 19**, various microstructures are available in CAD to modify the heating surface conditions. Various nano-textures are also superposed onto each specified microstructure surface. These micro-/nano-textures are aligned with different regularity in their topological design. For an example, the micro-/nano-textures are considered in trial to improve the coefficient of K_q at B′ in **Figure 18**. The hydrophilic or super-hydrophilic micro-textures with high peak-to-valley intensity ratio are suitable to attain much higher heat penetration rate by improving the surface properties of specimen-2.

Manufacturing to boiling heat transfer devices. In addition to the scientific understanding on the effect of micro-/nano-textures to the boiling heat transfer, how to make mass production of the textured heat-transfer devices must be also taken into account. In this chapter, two methods were proposed to build up the micro-textured devices. In the former method, a thick DLC-coating with more thickness than 20 μm was employed as a mother die to build up the tailored micro-/nano-textures by the plasma-oxidation-assisted printing. This die with the aligned micro-pillared punches was indented into the metallic work sheet to form the micro-cavity micro-textures on it. This plasma-oxidation-assisted technique is exchanged with other approaches. As demonstrated in [40–43], the nitrogen supersaturated stainless steels as well as this DLC coating are also utilized to make micro-/nano-texturing via the pico-/femto-second laser micromachining. The LIPSS (laser-induced periodical surface structured) nano-textures are precisely imprinted to metal plates and sheets by CNC-stamping. Through this precise stamping, the mother topology of micro-/nano-structures is imprinted onto the aluminum and copper device surfaces together with their engineering functions such as their grating in colors and surface plasmonic brilliance.

The latter method is a coating procedure including the dry and wet plating to form the micro-/nano-textures directly onto the metallic substrates. As shown in the acicular micro-texture formation in **Figures 12** and **13**, the anisotropic deposition of Fe–Ni alloy layers or the etching of deposited layers played a key process to control the unit cell size of the convex and concave micro-textures. Their topological alignment of each unit cell is also controllable in this approach. In application of these micro-textured devices to practical heat transferring system, they must be post-treated to have high hardness and strength against the erosion by the vapor bubble attack. Once these micro-/nano-texture layers are hardened and strengthened, the heat-transferring device surface can be functionally decorated by the tailored coating with complex topology.

5. Conclusion

The boiling heat transfer process with two-phase coolant flow has been utilized in various engineering fields including the heat exchanging facilities, the heat-spreading

devices of waste heats, or the high-cooling-rate equipment. Their design base stands on the classical knowledge of heat transfer mechanism through the flat metallic interface. The present study experimentally demonstrates that micro- and micro-/nano-texturing on the metallic interface can control the boiling heat transfer between the flowing coolant and the heated solid. The ultra-fine bubbles nucleate and take off with the coolant flow on the pure aluminum sheet and plate with regular alignment of micro-cavities. In addition to fine vapor bubbling in nucleation, these fine bubbles flow away with coolant without swelling onto the interface. Owing to this easy and prompt taking-off of bubbles, the heating interface is continuously wetted by fresh coolant to sustain the high heat flux through the micro-textured interface. This finding teaches the important role of fine bubble density and its dynamics in the nucleation step of boiling.

The heat flux to superheat relationship or the boiling curve is essential in the boiling heat transfer. It is much improved by the present micro-/nano-texturing. The onset superheat for transition from the convection heat transfer to the boiling nucleation is much reduced by homogeneous nucleation of bubbles with high density. With increasing the superheat over this onset, the heat flux increases in steep gradient. In addition, this steep increase of heat flux is much enhanced with increasing the coolant velocity. In classics, the boiling heat transfer has been believed never to be dependent on the coolant velocity. The high-speed camera observation in the present experiments discovers that the mass of two-phase local flow with fine bubbles takes off from the textured interface and moves away to the downstream of forced turbulent coolant flow. Since the fresh coolant flows onto the textured surface, the higher heat flux is sustained on the textured heating interface. This significant change of physical models in the boiling curve by micro-texturing suggests that multi-scaled physics are necessary to describe the microscopic heat transfer on the bubble nucleation, to analyze the mesoscopic interaction of vapor bubbles and fresh coolant flow, and to modify the macroscopic relationship between the heat flux and the superheat.

The present study started to consider the micro-/nano-textures tailored for each boiling heat transfer design. Much more scientific idea and engineering effort is still necessary to find a way to attain the much higher heat flux than the CHF in the heat exchanger, the heat pipes, the heat spreaders, and the thermal device to efficiently release the waste heat. A graphene with much higher thermal conductivity becomes a candidate to be working instead of metals for small-scaled cooing devices. The micro-/nano-textured sheet is near-net-shaped to a channel or a pipe with textured inner surfaces for highly efficient heat transferring and exchanging systems. The unit cell size and geometric topology are much modified to improve the convection heat transfer together with the boiling transfer [44]. The regularity in the alignment of unit cells in micro-/nano-texturing is further controlled to discuss the simultaneous nucleation and taking-off at the early stage of bubble nucleation.

Acknowledgements

The authors would like to express their gratitude to Dr. T. Yamada, Mr. M. Tasaka, and Mr. S. Suwa (Graduate School of Science and Engineering, SIT), and Mr. S. Kurozumi (Nano-Film Coat, llc.) for their help in experiments.

Conflict of interest

Authors declared no conflict of interests.

Nomenclature

q	Heat flux
q_{cr}	Critical heat flux (CHF)
ΔT	Superheat, the difference between wall temperature and saturation temperature
ΔT_{onset}	Superheat to onset for nucleation
ΔT_i	Intrinsic superheat
K_q	Heat penetration factor
h	Heat transfer coefficient
P	Power applied to heater
Re	Reynolds number
Pr	Prandle number
Nu	Nusselt number
u^*	Friction velocity
λ	Friction factor
u	Velocity of coolant
ρ	Mass density of coolant
ν	Viscous velocity
$y+$	Wall coordinate
κ	Thermal conductivity
θ	Static contact angle

Author details

Tatsuhiko Aizawa[1*], Naoki Ono[2] and Hiroki Nakata[3]

1 Surface Engineering Design Laboratory, Shibaura Institute of Technology, Tokyo, Japan

2 Shibaura Institute of Technology, Tokyo, Japan

3 Ebina Denka Kogyo, Co., Ltd., Tokyo, Japan

*Address all correspondence to: taizawa@sic.shibaura-it.ac.jp

References

[1] Tickerman DB, Pease RFW. High-performance heat sinking for VLSI. IEEE Electron Device Letters. 1981;**EDL-2**(5): 126-129

[2] Gong L, Zhao J, Huang S. Numerical study on layout of micro-channel heat sink for thermal management of electric devices. Applied Thermal Engineering. 2015;**88**:480-490

[3] Huang S, Zhao J, Gong L, Duan X. Thermal performance and structure optimization for allotted microchannel heat sing. Applied Thermal Engineering. 2017;**115**:1266-1276

[4] Li P, Luo Y, Zhang D, Xie Y. Flow and heat transfer characteristics and optimization study on the water-cooled microchannel heat sinks with dimple and pin-fin. International Journal of Heat and Mass Transfer. 2018;**119**: 152-162

[5] Milica L, Milan P, Vladimir S. Boiling heat transfer modeling: A review and future prospectus. Thermal Science. 2018;**23**:249-272

[6] Chang JY, You SM. Enhanced boiling heat transfer from micro-porous surfaces: Effects of a coating composition and method. International Journal of Heat and Mass Transfer. 1997; **40**(18):4449-4460

[7] Kattoh Y. Fundamentals in Heat Transfer. Yokendo; 1964

[8] Sodtke C, Stephan P. Spray cooling on micro structured surfaces. International Journal of Heat and Mass Transfer. 2007; **50**:4089-4097

[9] Hendricks TJ, Krishnan S, Choi C, Chang C-H, Paul B. Enhancement of pool-boiling heat transfer using nanostructure surface on aluminum and copper. International Journal of Heat and Mass Transfer. 2010;**53**:3357-3365

[10] Ahn HS, Lee C, Kim H, Jo H, Kang S-H, Kim J, et al. Pool boiling CHF enhancement by micro/nanoscale modification of zircaloy-4 surface. Nuclear Engineering and Design. 2010; **240**:3350-3360

[11] Jo H, Ahn HS, Kang S-H, Kim MH. A study of nucleate boiling heat transfer on hydrophilic, hydrophobic and heterogeneous wetting surfaces. International Journal of Heat and Mass Transfer. 2011;**54**:564305652

[12] Jung SM, Preston DJ, Jung HY, Deng Z, Wang EN, Kong J. Porous Cu nanowire aerosponges from one-step assembly and their applications in heat dissipation. Advanced Materials. 2016; **28**:1413-1419

[13] Simitses GJ, Hodges DH. Fundamentals of Structural Stability. Butterworth Heinemann; 2006

[14] Amon CH, Murthy J, Yao SC, Narumachi S, Wu C-F, Hsieg C-C. MEMS-enabled thermal management of high-heat-flus devices EDIFICE; embedded droplet impinging for integrated cooling of electronics. Experimental Thermal and Fluid Science. 2001;**25**(5):231-242

[15] Hamidnia M, Luo Y, Li Z, Wang X. Capillary and thermal performance enhancement of rectangular grooved micro heat pipe with micro pillars. International Journal of Heat and Mass Transfer. 2020;**153**:119581

[16] Aizawa T, Tamaki M, Fukuda T. Large area micro-texture imprinting

onto metallic sheet via CNC stamping. Journal of Procedia Engineering. 2014; **81**:1427-1432

[17] Aizawa T, Fukuda T. Pulsewise-motion controlled stamping for micro-texturing onto aluminum sheet. Journal of Micro- and Nano Manufacturing. ASME. 2016;**4**:014502-014511

[18] Aizawa T. Micro-Texturing for Tribology and Surface Engineering in Manufacturing Process. Proceedings of the 4th ISAST Conference, Indonesia; 2016. pp. 1-17

[19] Aizawa T, Suga H, Yamaguchi T. Plasma-nitriding assisted micro-texturing into stainless steel molds. Proceedings of the 4th ICNFT. 2015: 9002/1-9002/6

[20] Aizawa T, Takashima T, Shiratori T. Plasma printing to fabricate the micro-piercing dies for miniature metal products. Proceedings of the 8th AWMFT. 2015:J1/1-J1/6

[21] Nagata T, Aizawa T. Plasma-nitriding assisted modification of stainless steels for micro surgery knives. Proceedings of the 11th ICOMM. 2016;**59**:1-5

[22] Aizawa T, Inohara T. Pico- and femtosecond laser micromachining for surface texturing. Ch. 1. In: Micromachining. London UK: IntechOpen; 2019. pp. 1-24

[23] Hasegawa T, Aizawa T, Inohara T, Yoshihara S-I. Mold-stamping of optical glasses by micro/nano-textured die to transcript the hydrophobicity. J. Japan Society of Technology of Plasticity. 2019; **60**:23-27

[24] Aizawa T, Inohara T, Wasa K. Femtosecond laser micro-/nano-texturing of stainless steels for surface property control. Journal of Micromachines. 2019;**10**(512):1-10

[25] Aizawa T, Fukuda T. Oxygen plasma etching of diamond-like carbon coated mold-die for micro-texturing. Surface and Coating Technology. 2013;**215**: 364-368

[26] Aizawa T. Micro-texturing onto amorphous carbon materials as a mold-die for micro-forming. Applied Mechanics and Materials. 2014;**289**:23-37

[27] Yunata EE, Aizawa T. Micro-grooving into thick CVD diamond films via hollow cathode. Manufacturing Letters. 2016;**4**:17-22

[28] Shiratori T, Aizawa T, Saito Y, Wasa K. Plasma printing of an AISI316 micro-meshing punch array for micro-embossing onto copper plates. Journal of Metals. 2019;**9**(396):1-11

[29] Aizawa T, Saito Y, Hasegawa H, Wasa K. Fabrication of optimally micro-textured copper substrates by plasma printing for plastic mold packaging. International Journal of Automation Technology. 2020;**14**(2):200-207

[30] Aizawa T. Development of micro-manufacturing by controlled plasma technologies. J. Japan Society of Technology of Plasticity. 2017;**58**: 1064-1068

[31] Aizawa T, Yoshihara S-I. Microtexturing into AISI420 dies for fine piercing of micropatterns into metallic sheets. J. Japan Society of Technology of Plasticity. 2019;**60**:53-57

[32] Aizawa T, Inohara T, Wasa K. Fabrication of super-hydrophobic stainless steel nozzles by femtosecond laser micro-/nano-texturing.

International Journal of Automation Engineering. 2020;**14**(2):159-165

[33] Aizawa T, Shiratori T, Yoshino T, Inohara T. Femtosecond laser trimming of CVD-diamond coated punch for fine embossing. Materials Transactions. 2020;**61**(2):244-250

[34] Aizawa T, Shiratori T, Kira Y, Inohara T. Simultaneous nano-texturing onto CVD-diamond coated piercing punch with femtosecond laser trimming. Journal of Applied Sciences. 2020; **10**(2674):1-13

[35] Aizawa T, Ono N. Boiling heat transfer control by micro–/nano-texturing of metallic heat-spreading devices. In: Proc. 3rd WCMNM-2021. Mumbai, India; September 21st, 2021 (in press)

[36] Aizawa T, Wasa K, Tamagaki H. A DLC-punch array to fabricate the micro-textured aluminum sheet for boiling heat transfer control. Journal of Micromachines. 2018;**9**(147):1-10

[37] Aizawa T, Gregorius A, Ono N. Boiling heat transfer on the micro-textured copper interface. Journal of Micromachines. 2022 (in press)

[38] Tani I. The flow close to the wall of a turbulent boundary layer. Japan Journal of Aerospace and Aeronautics Society. 1973;**21**(228):39-43

[39] JSME. Heat Transfer Data Handbook. JSME; 2009

[40] Aizawa T, Yoshino T, Inohara T. Micro–/nano-texturing of aluminum by precise coining for functional surface decoration. Journal of Metals. 2020; **10**(1044):1-10

[41] Aizawa T, Inohara T, Wasa K. Nano-texturing onto tool-surface by the femtosecond laser processing. In: Proceedings of the WCMNM-2021. India, Mumbai; September, 2021 (in press)

[42] Aizawa T, Yoshino T, Shiratori T, Inohara T. Femtosecond laser printing of micro–/nano-textures into DLC dies for functional decoration of light metals. Journal of Nanomaterials. 2021 (in press)

[43] Aizawa T, Yoshino T, Suzuki Y, Komatsu T, Inohara T. Micro–/nano-texture surface decoration of metals and metallic alloys via femtosecond laser processing and precise imprinting. In: Proceedings of the 13th AFGS. China, Hong Kong; 2021. pp. 79-86

[44] Aizawa T, Nakata H, Nasu T. Manufacturing and characterization of acicular Fe-Ni micro-textured heat-transferring sheets. In: Proceedings of the 5th WCMNM Conference. Leuven, Belgium; September, 2022 (in press)